Internal Distribution of the Local SAR in the Human Abdomen Measured by a Split Phantom and Small Helical Antennas at 150 MHz

Yoshio KOYANAGI[*1&2], Hiroki KAWAI[2], Koichi OGAWA[3], Koichi ITO[4]
[1]R & D Center, Panasonic Mobile Communications Co., Ltd.
5-3 Hikarinooka, Yokosuka-shi, 239-0847, Japan koyanagi.yoshio@jp.panasonic.com
[2]Graduate School of Science and Technology, Chiba University
[3]Devices Development Center, Matsushita Electric Industrial Co., Ltd.
[4]Department of Urban Environment Systems, Faculty of Engineering, Chiba University

1. INTRODUCTON

In the 150 MHz portable radio terminals that are now frequently used for business purposes, a normal mode helical antenna (NHA) with a short axial length is commonly utilized in a radio set attached to the human abdomen, as shown in Fig. 1. Thus, the antenna performance is strongly influenced by the effect of electromagnetic coupling between the antenna and the human body [1]. On the other hand, from the viewpoint of health hazards relating to the human body, an accurate evaluation of the Specific Absorption Rate, known as the SAR, is of particular interest [2].

At VHF frequencies, radio waves can penetrate into the human body more easily than they can at the UHF frequencies at which cellular radios operate. Therefore, a precise assessment of the internal SAR distribution in the human abdomen, in which there are a number of significant internal organs, is particularly important when we come to consider the EM-safety problem for the radios used in the VHF-band. The authors have studied the SAR distribution of an NHA as observed at the surface of a human abdomen using a cylindroid whole body phantom [2]. However, there have been few studies regarding the internal SAR distribution created by NHA's at 150 MHz.

The purpose of this paper is to analyze and measure the internal SAR distribution in a human abdomen created by portable radio terminal antennas at 150 MHz. To this end, we have developed a unique phantom that can be split into two pieces in the longitudinal direction along its center. A thermographic technique is used for the SAR measurement in the cut plane of the phantom. An analytical approach involving thermal analysis using the finite element method was conducted in conjunction with EM analysis by FDTD to estimate the cooling effects that occur by thermal diffusion in the phantom after exposure to EM energy.

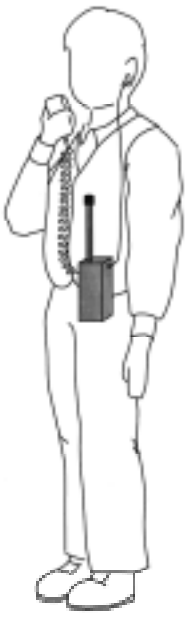

Fig.1 Business portable radio in a talk situation.

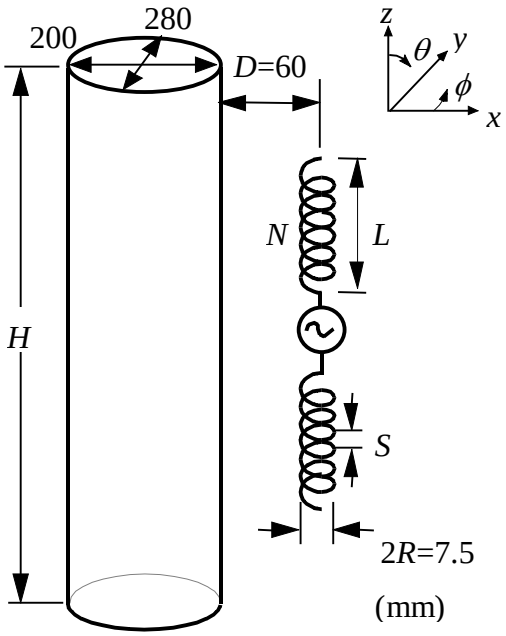

Fig.2 Analytical model.

2. ANTENNAS AND THE HUMAN BODY

Fig. 2 shows an NHA placed close to a model representative of a human body. The monopole NHA attached to the small radio box in Fig. 1 is replaced by a dipole-shaped NHA fed via a coaxial cable through a U-balun and a matching capacitor [1]. The NHA is conjugate- matched by a capacitor. Two antenna shapes (pitch S, number of windings N, and axial length $2L$) denoted as ANT1 and ANT2, were evaluated; the parameters of ANT1 are $2L$ = 204 mm (0.10λ), N = 98, S = 1.9 mm, and those of ANT2 are $2L$ = 356 mm (0.18λ), N = 99, S = 3.4 mm. The winding diameter is $2R$ = 7.5 mm and the diameter of the metal wire is 1 mm. The distance between the NHA and the surface of the human model was set as D = 60 mm with reference to the monopole NHA used in practice for 150 MHz business portable radios.

The human model has an elliptical cross section with a major axis of 280 mm (0.14λ) and a minor axis of 200 mm (0.10λ), which were intended to represent to the body shape of average Japanese youths in their twenties [3]. The phantom has electrical parameters of ε_r = 42.1, σ = 0.514 S/m, and ρ = 907 kg/m^3, where ε_r is the relative permittivity, σ is the conductivity and ρ is the density, which were intended to represent the average values for human tissues [4].

3. ABDOMEN SPLIT PHANTOM

In a previous study [2], a whole body phantom of 1300 mm in height was used to measure the radiation and SAR characteristics. However, it is difficult to adopt a structure that can be split into two parts when using such a large size for the phantom. Hence, in the first stage of our investigation, we studied the required height of the phantom from the viewpoint of the SAR measurement.

Fig.3 shows the calculated results of the peak SAR values that we observed at the surface of the phantom as a function of the phantom height H. It can be seen from Fig.3 that the peak SAR changes by less than 3 % as the height H changes from 500 to 1700 mm, indicating that a phantom with H = 500 mm can be used for the purposes of SAR assessment of the NHA evaluated in this paper. Taking this into consideration, an abdomen phantom with H = 500 mm was constructed.

Fig. 4 shows an external view of the abdomen phantom, which can be separated into two pieces in the longitudinal direction. The principal constituent of the model is glycerin [5]. The two halves of the phantom are integrated into one single piece when the exposure to EM power takes place and are then split back into two pieces after the exposure to observe the temperature rise using an infrared camera [2].

4. THERMAL ANALYSIS

When using the thermographic method, the exposure time needs to be sufficiently long that an adequate temperature rise can be obtained deep inside the 'body' of the phantom at 150 MHz. However, this long exposure results in a phenomenon where the heated phantom is already cooling due to thermal diffusion and conduction. Therefore, in order to make an accurate measurement of the internal SAR distribution, the

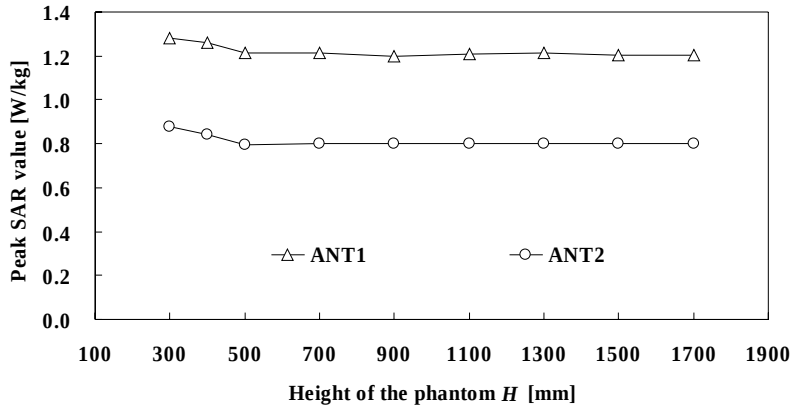

Fig.3 Local SAR near the feed point of NHA vs. height of the phantom H.

Fig.4 Abdomen split phantom.

effect of this temperature decrease on the SAR evaluation has been characterized by a thermal analysis technique using ANSYS (ver. 6.0).

Fig. 5 shows the analytical results of the temperature rise ΔT in the phantom with exposure power and time as parameters. The three kinds of exposure conditions in Fig. 5 were chosen such that the power-time product remains constant for the respective antenna. In Fig. 5 the curves represented by the 'X' symbols indicate the case where there is no thermal diffusion or conduction. The thermographic method commonly uses this condition to obtain the SAR.

It can be seen from Fig. 5 that a greater decrease in temperature occurs in the region between 0 and 10 mm from the phantom surface as the exposure time Δt becomes longer. For example, for ANT1 the maximum ΔT in the case of Δt = 120 sec is 4.2 K, which is 11 % lower than the ΔT of 4.7 K for the case where there is no thermal diffusion and conduction. Similarly, for ANT2 the maximum ΔT in the case of Δt = 180 sec is 4.1 K, which again is 13 % lower than when there is a ΔT of 4.7 K. Under these Δt conditions, we can also see from Fig. 5 that there is no appreciable decrease in the temperature in the interior region of the phantom deeper than 5 mm from the surface. Therefore a Δt of 120-180 sec was chosen for the exposure condition in the experiments.

5. EXPERIMANTAL RESULTS

Fig. 6 shows the SAR distribution in the *x*-*z* plane. The measured and calculated results are in quite good agreement. The conduction loss due to the metal wire of the antenna was calculated to be 24 % for ANT1 and 10 % for ANT2 [1]. Hence, the radiation power was adjusted to be 1 W in the analysis in Fig. 6. As a result, the measured and calculated peak SAR values agree very well, as shown in Fig. 6. This suggests that when evaluating small antennas, the conduction loss of the antenna should be included in the analysis for an accurate SAR assessment.

Fig. 7 shows that the SAR distribution inside the phantom along the *x*-axis. The measured results agree very well with the calculated results. There is a maximum value near the surface of the phantom and no local peak point greater than the maximum inside the phantom. In Fig.7, one important consideration is that the SAR value at 50 mm from the phantom surface, where a number of significant internal organs are considered to exist, is as small as 0.24 W/kg for ANT1 and 0.17 W/kg for ANT2 when the radiated power was 1 W. These values are small in comparison with the safety limits regulated by national and international organizations [6]. However, a commercial business radio has a maximum power of 5 W, and thus it is predicted from the results obtained in Fig. 7 that the SAR becomes nearly 1 W/kg, which is still less than the safety limit but which cannot be ignored because it leaves less tolerance.

Although a homogeneous phantom structure is used in this paper, there are various kinds of organs in the actual human abdomen that have different electrical parameters. In such a situation, there is a possibility that a particular organ may have a higher SAR than the SAR value evaluated by the homogeneous phantom in this paper. This is left for further studies.

REFERENCES

[1] K. Ogawa, Y. Koyanagi and K. Ito: " An Analysis of the Effective Radiation Efficiency of the Normal Mode Helical Antenna Close to the Human Abdomen at 150 MHz and Consideration of Efficiency Improvement," Electronics and Communications in Japan, Part I, vol. 85, no. 8, pp. 23-33, 2002.

[2] Y. Koyanagi, H. Kawai, K. Ogawa, H. Yoshimura, and K. Ito: "Estimation of the Radiation and SAR Characteristics of the NHA at 150 MHz by Use of the Cylindroid Whole Body Phantom," IEEE AP-S Intl. Symp. Digest, pp. 78-81, July 2001.

[3] Agency of Industrial Science and Technology, National Institute of Bioscience and Human-Technology, "Japanese body size data base for the design," Reports from National Institute of Bioscience and Human-Technology, 2, 1, 1994.(in Japanese)

[4] A. W. Guy, C. Chou, and B. Neuhaus, "Average SAR and SAR Distributions in Man Exposed to 450-MHz Radiofrequency Radiation," IEEE Trans. MTT, MTT-32, No. 8, pp. 752-762, Aug. 1981.

[5] Y. Okanao, K. Ito, and H. Kawai, "Solid phantom composed of glycerin and its application to SAR estimation," Trans. of IEICE, vol. J83-B, no. 4, pp. 534-543, Apr. 2000.(in Japanese)

[6] IEEE standard for safety levels with respect to human exposure to radio frequency electro- magnetic fields, 3 kHz to 300 GHz, IEEE Std C95-1-1991, Apr. 1992.

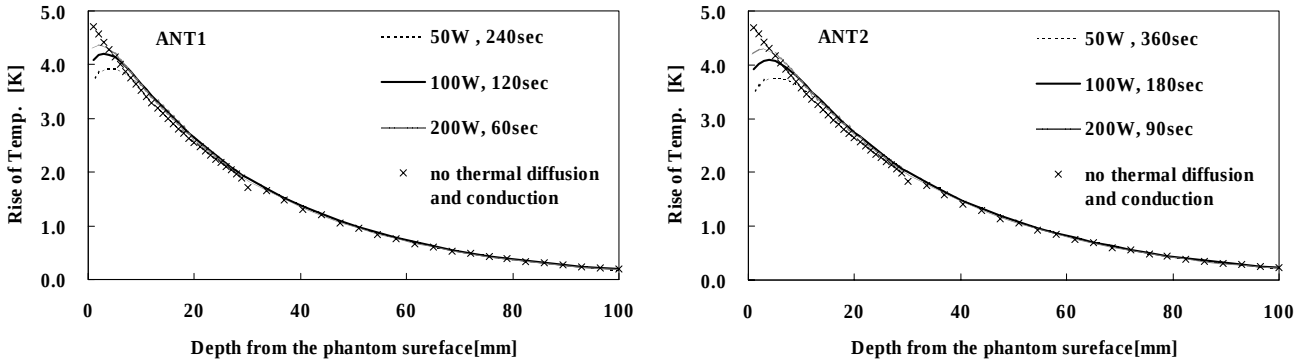

Fig.5 ΔT distributions in the phantom vs. radiation conditions.

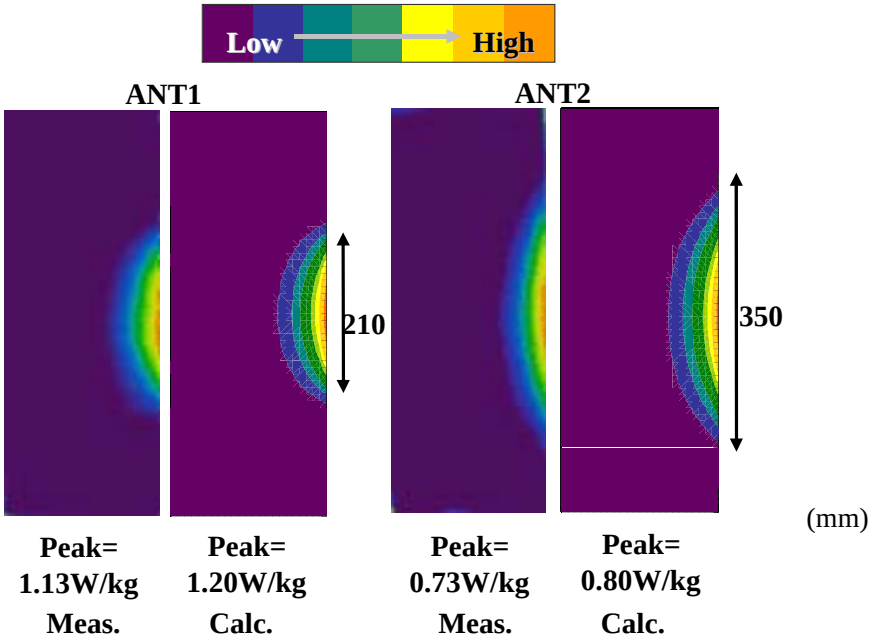

Fig.6 SAR distributions in the phantom.

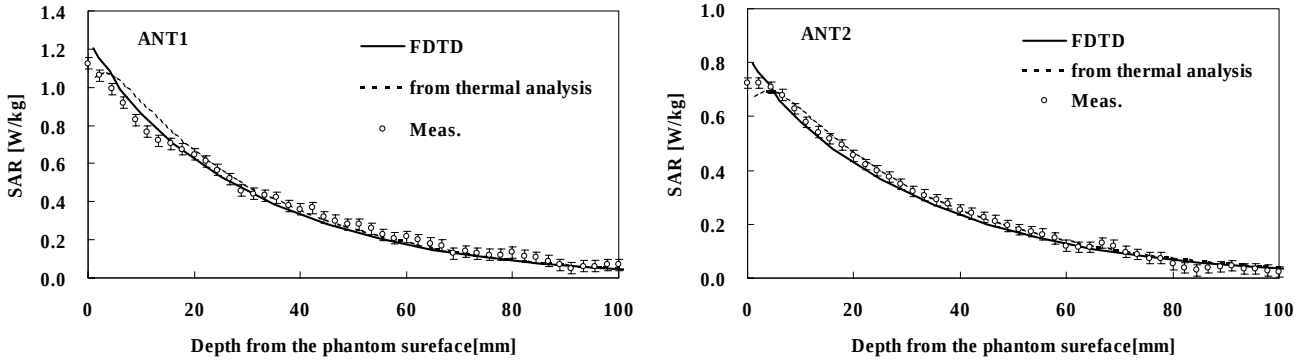

Fig.7 SAR distributions in the phantom along the *x*-axis.